Cytotoxic necrotizing factor 1 promotes bladder cancer angiogenesis through activating RhoC

Yaxiu Guo,[1#] Jingyu Wang,[1#] Kaichen Zhou,[1] Junqiang Lv,[1] Lei Wang,[2] Shan Gao,[2] Evan T. Keller,[3] Zhi-Song Zhang,[2]* Quan Wang,[1]* Zhi Yao[1,4]*

[1]Department of Immunology, Key Laboratory of Immune Microenvironment and Disease of the Educational Ministry of China, Tianjin Key Laboratory of Cellular and Molecular Immunology, School of Basic Medical Sciences, Tianjin Medical University, Tianjin 300070, China.

[2]State Key Laboratory of Medicinal Chemical Biology and College of Pharmacy, Collaborative Innovation Center for Biotherapy, and Tianjin Key Laboratory of Molecular Drug Research, Nankai University, Tianjin 300350, China.

[3] Departments of Urology, University of Michigan, Ann Arbor, Michigan, USA.

[4]2011 Collaborative Innovation Center of Tianjin for Medical Epigenetics, Tianjin Medical University, Tianjin 300070, China.

[#]These authors contributed equally to this study.

***Corresponding Author:** Zhi Yao, Tianjin Medical University; Tel.: 86-22-83336817; E-mail address: yaozhi@tmu.edu.cn; or Quan Wang, Tianjin Medical University; Tel.: 86-22-83336817; E-mail address: wangquan@tmu.edu.cn; or Zhi-Song Zhang, Nankai University; Tel.: 86-22-85358010; E-mail address: zzs@nankai.edu.cn

The authors declare no conflict of interest.

Running title: CNF1 promotes bladder cancer angiogenesis.

Keywords: Uropathogenic *Escherichia coli*; cytotoxic necrotizing factor 1; RhoC; bladder cancer; angiogenesis.

Nonstandard Abbreviations

qRT-PCR, quantitative real-time reverse transcription polymerase chain reaction;

Co-IP, Co-immunoprecipitation;

RPMI, Roswell Park Memorial Institute;

PBS, phosphate-buffered saline;
ELISA, Enzyme-linked immunosorbent assay;
HRP, horseradish peroxidase;
PEI, polyethylenimine;
OCT, optimum cutting temperature;
IHC, Immunohistochemistry;
H&E, hematoxylin and eosin;
FITC, fluorescein isothiocyanate;
DAPI, 2-(4-amidinophenyl)-1H-indole-6-carboxamidine;
ANOVA, analysis of variance.

Abstract

Uropathogenic *Escherichia coli* (UPEC), a leading cause of urinary tract infections, is associated with prostate and bladder cancers. Cytotoxic necrotizing factor 1 (CNF1) is a key UPEC toxin; however, its role in bladder cancer is unknown. In the present study, we found CNF1 induced bladder cancer cells to secrete vascular endothelial growth factor (VEGF) through activating Ras homolog family member C (RhoC), leading to subsequent angiogenesis in the bladder cancer microenvironment. We then investigated that CNF1-mediated RhoC activation modulated the stabilization of hypoxia-inducible factor 1α (HIF1α) to upregulate VEGF. We demonstrated *in vitro* that active RhoC increased heat shock factor 1 (HSF1) phosphorylation, which induced heat shock protein 90α (HSP90α) expression, leading to stabilization of HIF1α. Active RhoC elevated HSP90α, HIF1α, VEGF expression, and angiogenesis

in the human bladder cancer xenografts. In addition, HSP90α, HIF1α and VEGF expression were also found positively correlated with human bladder cancer development. These results provide a potential mechanism through which UPEC contributes to bladder cancer progression, and may provide potential therapeutic targets for bladder cancer.

Introduction

Uropathogenic *Escherichia coli* (UPEC) induced urinary tract infections (UTIs) usually evoke cystitis, pyelonephritis, and prostatitis (1-3). In addition, UPEC was also reported to accelerate prostate cancer progression in the genetically engineered Hi-Myc mouse prostate cancer model, and increase the risk of bladder cancer through promoting CDKN2A methylation (4, 5). Previously, we reported that cytotoxic necrotizing factor 1 (CNF1), a key UPEC toxin, promoted migration and invasion of prostate cancer cells and prostate cancer metastasis by activating the Cdc42-PAK1 Axis (6). Although UPEC frequently infects bladder, the role of CNF1 in bladder cancer has not been reported.

CNF1 binds to cells through a specific receptor, enters the cytosol, and then activates Rho GTPases (including RhoA, Cdc42 and Rac1) by deamidation of specific glutamine residues (7). RhoA, RhoB and RhoC belong to the same subfamily of Rho GTPases based on phylogenetic analysis (8), and the expression or activity of RhoA and RhoC are increased in many types of human tumors (9, 10). RhoC has been reported to facilitate the invasion and metastasis of tumor cells (11) and promote tumor angiogenesis by inducing the release of vascular endothelial growth factor

(VEGF) (12). However, the mechanism by which RhoC induces VEGF is unclear.

Angiogenesis is essential for tumor progression and is highly dependent on VEGF (13), which is expressed by most of the malignant tumors (14, 15). Under hypoxic conditions, hypoxia-inducible factor 1 (HIF1) induces the transcription of VEGF (16). HIF1 is a heterodimeric transcription factor composed of a constitutively-expressed HIF1β-subunit and an O_2-regulated HIF1α subunit, and is a major regulator of angiogenesis in the tumor microenvironment (17, 18).

Under normoxic conditions, HIF1α can be hydroxylated at critical proline residues by dioxygenase prolyl hydroxylases, and degraded through pVHL mediated ubiquitin-proteasome pathway (19, 20). However, under hypoxic conditions, the activity of dioxygenase prolyl hydroxylases is suppressed, and HIF1α is stable (21). In addition, HIF1α degradation can be decreased by several pVHL-independent mechanisms (22, 23). For example, the heat shock protein 90 (HSP90), a molecular chaperone, has been reported to stabilize HIF1α by binding it directly (22). The role and mechanism of RhoC in regulating HIF1α has not been reported.

In this study, we examined if and how CNF1 facilitated VEGF secretion by tumor cells and the subsequent angiogenesis in the bladder cancer microenvironment. We found that CNF1 induced VEGF and angiogenesis through RhoC-dependent activation of the HSF1-HSP90α-HIF1α axis. These results may provide potential bladder cancer therapeutic targets.

Materials and methods

Cell lines

The T24, 5637, UMUC3, and 293T cells were obtained from the ATCC (Manassas, VA, USA). The HUVECs were a generous gift from Dr. Zhi-Song Zhang from the College of Pharmacy, Nankai University, Tianjin, China. For hypoxic conditions, the cells were cultured in a modular incubator chamber flushed with mixed gas consisting of 1% O_2, 5% CO_2, and 94% N_2 at 37 ℃. For normoxic conditions, mixed gas consisting of 20% O_2, 5% CO_2, and 75% N_2 at 37 ℃ was used. Other reagents used included the HSF1 inhibitor KRIBB11 (S8402; Selleck Chemicals, Houston, TX, USA); the NF-κB inhibitor BAY 11-7085 (HY-10257; MedChem Express, Monmouth Junction, NJ, USA); and the proteasome inhibitor MG132 (M7449; Sigma-Aldrich, St. Louis, MO, USA).

Plasmids

The *cnf1* gene from UPEC strains 11 was amplified by PCR and cloned into pET-28a(+) (Novagen, Madison, WI, USA). The coding sequences for RhoC, HIF1α, and HSP90α were subcloned into pCMV-Tag2B (Stratagene, La Jolla, CA, USA), pLVX-EF1α-IRES-Puro, pLVX-IRES-Hyg (Clontech, Mountain View, CA, USA) or pCDNA3.1-HA-Hygro (Invitrogen, Carlsbad, CA, USA). The constructed plasmids and primer sequences are listed in supplementary Table 1 and Table 2.

CNF1 recombinant protein expression and purification

Recombinant proteins of CNF1 and its mutant C866S were expressed, purified and identified as described previously (6).

Mutagenesis

Mutagenesis of *cnf1* and RhoC was performed using a Fast Mutagenesis System kit (TransGen Biotech, Beijing, China) according to the manufacturer's protocol. The primers used for mutation are listed in supplementary Table 2.

Transwell migration and invasion assays

Cell migration and invasion assays were performed using Transwell chambers (pore size 8 μm, Costar, Corning 3422), with Corning Matrigel Matrix (Corning Incorporated, Corning, NY, USA) for invasion assays. Cells (1×10^5 in 200 μL) resuspended in serum-free RPMI 1640 medium were added to the upper chamber of

uncoated (for migration assays) or Matrigel-coated (for invasion assays) membranes with PBS, CNF1 (1 nmol/L), or C866S (1 nmol/L). Then, 600 μL of medium containing 20% fetal bovine serum with according PBS, CNF1 (1 nmol/L), or C866S (1 nmol/L) was added to the lower chamber. After 12 h (migration assays) or 24 h (invasion assays) incubation at 37 ℃ in a 5% CO_2 humidified atmosphere, the cells that adhered to the bottom surface of the inserts were fixed in 4% paraformaldehyde for 1 h and stained with 0.1% crystal violet (Beijing Solarbio Science & Technology Co. Ltd., Beijing, China) for 15 min. Finally, the filters were washed three times in PBS and images were captured under a microscope (Leica Microsystems, Wetzlar, Germany) at 200 × magnification.

Gelatin zymography assay

The activities of MMP2 and MMP9 were analyzed by gelatin zymography as described previously (24). In brief, cells were incubated with serum-free medium supplemented with PBS or CNF1 (1 nmol/L) for 24 h at 37 ℃. The conditioned medium was collected and mixed with β-mercaptoethanol-free sample loading buffer without boiling, and then electrophoresed on 10% (w/v) SDS-PAGE containing 0.1% (w/v) gelatin (Sigma- Aldrich). After electrophoresis, the gels were washed for 30 min with 2.5% (v/v) Triton X-100 (Merck Millipore, Billerica, MA, USA) to remove SDS and then incubated overnight at 37 ℃ in developing buffer (50 mmol/L Tris, pH 7.8, 5 mmol/L $CaCl_2$). Bands corresponding to the enzyme were visualized by staining with 0.2% (w/v) Coomassie brilliant blue R-250 (Merck Millipore), 50% (v/v) methanol, and 10%(v/v) acetic acid. The activities of MMP2 and MMP9 were quantified using ImageJ and β-Actin was detected using western immunoblotting as an internal control.

ELISA assay

Human bladder cancer cells were seeded in 12-well culture plates and incubated with serum-free medium supplemented with PBS, CNF1 (3 nmol/L), or CNF1 mutant C866S (3 nmol/L) for the indicated times at 37 ℃ under normoxic or hypoxic conditions. The medium was removed and stored at –80 ℃ until the assay was performed. VEGF in the medium was assayed using the Human VEGF Mini ABTS

ELISA Development Kit (PeproTech, Rocky Hill, NJ, USA), according to the manufacturer's instructions.

Tube formation assay

T24 and 5637 cells were cultured in serum-free RPMI 1640 supplemented with PBS or CNF1 (3 nmol/L) for 36 h. The conditioned media were collected separately, centrifuged, and stored at –80 ℃. Growth factor-reduced Matrigel (BD Biosciences, Bedford, MA, USA) was dissolved at 4 ℃ and 96-well plates were prepared with 50 μL of matrigel in each well after coating and incubating at 37 ℃ for 1 h. HUVECs (1×10^4) were suspended in 100 μL of conditioned medium. After 6 h of incubation at 37 ℃, HUVECs tube formation was assessed using a photomicroscope, and each well was photographed at 100 × magnification under a light microscope. The total length of the tubes was analyzed using the ImageJ software.

RNA isolation and qRT-PCR

Total RNA was isolated using the Trizol reagent (Beijing Solarbio Science & Technology Co. Ltd.). Total RNA (2 μg) was used to synthesize first-strand cDNA using M-MuLV reverse transcriptase (Thermo Fisher Scientific, Waltham, MA, USA). qRT-PCR was then performed using the SYBR green mix (Thermo Fisher Scientific). The reactions were performed with a LightCycler® 96 Real-Time PCR System (Roche, Basel, Switzerland). β-Actin was used as the endogenous control gene and the data were normalized based on the transcription level of β-Actin in the wild-type and quantified using the comparative critical threshold cycle $2^{-\Delta\Delta Ct}$ method. The primers used are listed in supplementary Table 2.

RNA sequencing (RNA-Seq)

After transfection with the vector or RhoC-Q63E, total RNA of T24 cells was extracted using the Trizol reagent. The RNA-Seq was performed by Majorbio (Shanghai, China). The data were analyzed on the free online platform of Majorbio I-Sanger Cloud Platform (www.i-sanger.com). The RNA-seq data are available under GEO accession GSE129295.

Antibodies and western blotting

Antibodies were ordered from the following companies: anti-HIF1α (20960-1-AP,

1:1000), anti-HSF1 (51034-1-AP, 1:1000), anti-RhoC (10632-1-AP, 1:1000), and anti-Myc (60003-2-Ig, 1:2000) were from Proteintech (Chicago, IL,USA); anti-HSF1 phosphorylated at Ser326 antibody (ab76076, 1:2000) was from Abcam (Cambridge, MA, USA); anti-HA (#3724, 1:1000), and anti-HSP90α (#8165, 1:1000) were from Cell Signaling Technology (Danvers, MA, USA); anti-RhoA (ARH04, 1:500) and anti-Rac1 (ARC03, 1:500) were from Cytoskeleton (Denver, CO, USA); anti-RhoB (sc-8048, 1:500) was from Santa Cruz Biotechnology (Santa Cruz, CA, USA); anti-Cdc42 (BA2442, 1:500) was from Wuhan Boster Biological Technology Co. Ltd. (Wuhan, China); and anti-Flag (F1804, 1:1000) was from Sigma-Aldrich. Cells were washed with PBS three times after treatment. Whole cell lysates were prepared using RIPA lysis buffer (Merck Millipore), with the addition of complete protease inhibitors (Roche). The protein concentration was determined using the BCA Protein Assay Kit (Thermo Fisher Scientific) and approximately 20 μg of cell lysates were used. Antibody binding was revealed using an HRP-conjugated anti-rabbit IgG or anti-mouse IgG (Sigma-Aldrich). Antibody complexes were detected using Immobilon Western Chemiluminescent HRP Substrate (Merck Millipore) and exposed in a Tanon-5200 machine.

Immunoprecipitation

Cells were lysed using lysis buffer containing 50 mmol/L Tris, pH 7.4, 150 mmol/L NaCl, 0.2 mmol/L EDTA, 1% NP-40, and protease inhibitors (Roche). The lysates were centrifuged at 14,000 rpm for 15 min at 4 ℃. The extracts were incubated with Anti-c-Myc Agarose (Sigma-Aldrich) overnight at 4 ℃. The beads were then washed exhaustively with the lysis buffer. Immobilized proteins were eluted with 2 × Laemmli sample buffer and subjected to SDS-PAGE.

RNA interference

Double-stranded RNAs as siRNAs for the targeted genes and scrambled siRNA (siScr) were synthesized by GenePharma (Shanghai, China). The sequences (sense strand) of the siRNAs are listed in supplementary Table 2. Specific gene knockdowns were assessed by western blotting. Transfection of siRNAs was carried out using Lipofectamine 3000 (Invitrogen).

Rho GTPase activation assays

T24 cells were seeded in 10-cm dishes. After treatment, RhoC activation was measured using a Rho Activation Assay Biochem Kit (BK036, Cytoskeleton) according to the manufacturer's protocol.

Transduction and transfection

T24 cells stably expressing RhoC constitutively active mutant Q63E were constructed using lentiviral supernatant. T24 cells were transiently transfected with the RhoC-related plasmids using Lipofectamine 3000 (Invitrogen). 293T cells were transiently transfected with the RhoC, HIF1α, and HSP90α-related plasmids using PEI (Sigma-Aldrich).

Xenograft model

All animal studies were reviewed and approved by the Animal Care and Use Committee at Tianjin Medical University, Tianjin, China. We made every effort to minimize animal suffering and to reduce the number of animals used. Six to eight-week-old female athymic BALB/c nude mice were purchased from the Academy of Military Medical Science (Beijing, China). T24 cells expressing RhoC mutant Q63E or the control were resuspended in 100 μL of PBS and injected into the flank of the nude mice (1×10^6 cells per animal). The xenografts were measured as described in figure legends. Then the tumor was collected and the volume and weight were measured. The tumors were fixed in 10% formalin or OCT compound for further analysis.

Immunohistochemistry (IHC)

Tumor samples were fixed in 10% formalin for 24 h and processed for paraffin embedding. Sections (5 μm) were used for H&E and IHC staining for RhoC (1:400, 10632-1-AP; Proteintech), HSP90α (1:300, 13171-1-AP; Proteintech), HIF1α (1:500, ab51608; Abcam), VEGF (1:300, 19003-1-AP; Proteintech). Images were acquired using an optical microscope (BX46, Olympus, Tokyo, Japan).

Tissue microarray analysis

The bladder cancer tissue microarray (BL2081c) containing 183 samples (8 of normal bladder tissue, 8 of adjacent normal bladder tissues, and 167 malignant tissues with

grade I, II or III) was purchased from Alenabio (Xi'an, China). The staining intensity values were determined by Image-Pro Plus software.

Immunofluorescence Analysis of Tissues

Tumor samples were embedded in OCT compound with liquid nitrogen. Frozen sections (5 μm) were used for immunofluorescence staining for CD31 (1:300, 550274; BD Biosciences) overnight at 4 ℃. After that, coverslips were washed with PBS, and incubated with FITC-labeled secondary antibody for 1 h. Finally tissue sections were counterstained with DAPI for nuclei visualization. Images were acquired under a fluorescence microscope (IX73, Olympus).

Statistical analyses

The statistical significance of the differences between groups were calculated using the two-tailed Student's *t*-test, non-parametric Mann-Whitney test, or ANOVA using SPSS 22.0 software (IBM Corp., Armonk, NY, USA).

Results

CNF1 promotes the migration and invasion of bladder cancer cells and vascular endothelial cells *in vitro*

We first examined effects of CNF1 on the migration and invasion abilities of bladder cancer cells. We purified and validated CNF1 and C866S (an inactive mutant of CNF1) recombinant proteins from UPEC strain as we previously described (6), and treated bladder cancer cell lines 5637 and T24. The Transwell assay showed that wild-type CNF1 markedly enhanced the migration and invasion of T24 and 5637 cells. (Fig. 1A and B, Supplementary Fig. 1A and B). The gelatinases (MMP2 and MMP9) play a pivotal role in degrading the extracellular matrix (ECM) (25). Accordingly, we explored whether the increased invasive effect could be attributed to MMP2 or MMP9 using a gelatin zymography assay. The results showed that MMP2 activity was increased in 5637 cells treated with CNF1 (Fig. 1C), and MMP9 activity was not detected in 5637 cells. Both MMP2 and MMP9 activity were not detected in T24 cells (data not shown). We further validated the effects of CNF1 on another bladder cancer cell line (UMUC3), which indicated that CNF1 enhanced MMP9 but not MMP2 activity (Supplementary Fig. 1C). Taken together, these results provide strong evidence that CNF1 promotes the migration and invasion of bladder cancer cells and that MMPs may contribute to this activity.

Endothelial cells are an important component of the microenvironment; therefore, we examined the impact of CNF1 on motility and invasiveness of human umbilical vein vascular endothelial cells (HUVECs). We found CNF1 promoted migration and invasion of HUVECs (Fig. 1D and E). Therefore, we speculated that CNF1 might have a synergistic effect on both cancer cells and angiogenesis.

CNF1 induces VEGF secretion in bladder cancer cells and subsequently promotes angiogenesis in HUVECs

VEGF is closely associated with tumor angiogenesis (26), and tumor cells are one of the main producers of VEGF in the tumor microenvironment. In addition, tissue hypoxia is a common feature of solid tumors (27). To determine whether CNF1 could

promote VEGF production from bladder cancer cells, we treated T24 or 5637 cells with CNF1, and determined VEGF secretion under normoxic and hypoxic conditions. CNF1 significantly promoted VEGF secretion from T24 and 5637 cells under hypoxic conditions, but not under normoxic conditions (Fig. 2A, Supplementary Fig. 2A). CNF1 promoted VEGF secretion in a time- and concentration-dependent manner in T24 and 5637 cells (Fig. 2B and C, Supplementary Fig. 2B and C).

Angiogenesis mainly involves endothelial cell migration and tube formation to form new blood vessels (28). Thus, we next examined whether CNF1-induced VEGF secretion stimulated angiogenesis in a HUVEC model *in vitro*. The results demonstrated that conditioned medium (CM) from CNF1-treated T24 and 5637 cells dramatically enhanced tube formation of HUVECs (Fig. 2D, Supplementary Fig. 2D). However, CNF1 did not play a direct role in promoting angiogenesis by itself (Supplementary Fig. 2E). These data suggest that CNF1 promotes angiogenesis by inducing VEGF secretion in bladder cancer cells.

Involvement of HIF1α in CNF1-induced VEGF secretion

We next explored the mechanism through which CNF1 induces VEGF expression. CNF1 markedly increased the VEGF mRNA level in T24 cells by qRT-PCR analysis (Fig. 2E). As a pivotal transcription factor, HIF1α is critical for VEGF transcription in tumor angiogenesis (29). Therefore, we investigated the possible effect of CNF1 on HIF1α. We treated T24 cells with CNF1 for 24 h and identified that CNF1 up-regulated the HIF1α protein level, but not its mRNA expression, compared with that in the control groups (Fig. 2F, Supplementary Fig. 3A). We also ruled out the possible role of LPS in inducing HIF1α (Fig. 2F). We then explored the mechanism by which CNF1 increases the protein levels of HIF1α. The addition of the proteasome inhibitor MG132 strongly blocked CNF1-mediated HIF1α upregulation under hypoxic conditions, suggesting that CNF1 promotes HIF1α upregulation in a proteasome-dependent manner (Fig. 2G). In addition, CNF1 effect on VEGF upregulation and increased tube formation of HUVECs was not detected in T24 and 5637 cells with HIF1A knockdown (Fig. 2H-J, Supplementary Fig. 2F and G). These results suggest that CNF1 increases the secretion of VEGF by increasing HIF1α accumulation.

CNF1 modulates the expression of HIF1α and the secretion of VEGF by activating RhoC

Rho GTPases are the main targets of CNF1 in mammalian cells (30). To determine if Rho GTPase play a role in CNF1-induced HIF1α upregulation, we knocked down expression of several Rho GTPase family members (RhoA, RhoB, RhoC, Rac1, and Cdc42) using siRNAs (Supplementary Fig. 3B). The CNF1-mediated increase of HIF1α protein levels was significantly attenuated by knockdown of RhoC compared with that achieved by siScr control, but not by knockdown of other Rho GTPases genes (Fig. 3A), which suggest that CNF1 upregulates HIF1α levels through RhoC. The role of RhoC in HIF1α upregulation induced by CNF1 was verified on another bladder cancer cell line 5637 (Supplementary Fig. 3C).

We then examined RhoC activation induced by CNF1. Treatment with CNF1 for 3 h caused a shift in the apparent molecular mass of RhoC on SDS–PAGE (Fig. 3B), indicating that the RhoC was covalently modified. We further validated the immunoblotting results using a pull-down assay (Fig. 3C). These results suggest that CNF1 can up-regulate the expression of HIF1α by inducing RhoC activation in bladder cancer cells.

To determine the role of active RhoC in the expression of HIF1α and the secretion of VEGF, wild-type RhoC (WT-RhoC, WT) or the constitutively active RhoC mutant (CA-RhoC, Q63E; Q63 was deamidated by CNF1 (7)) was transfected into T24 and 293T cells. Cells transfected with CA-RhoC had higher levels of HIF1α and their protein levels were significantly increased in a concentration-dependent manner compared with T24 and 293T cells transfected with vector or WT-RhoC (Fig. 3D, Supplementary Fig. 3D). However, transfection did not significantly increase the mRNA level of HIF1α (Supplementary Fig. 3E).

We further analyzed the possible effect of CA-RhoC on VEGF secretion. The results confirmed that overexpression of CA-RhoC effectively increased the secretion of VEGF compared with that in vector or WT-RhoC groups in T24 and 5637 cells (Fig. 3E, Supplementary Fig. 3F). In addition, transfection with RhoC siRNA inhibited CNF1-enhanced secretion of VEGF (Fig. 3F).

Taken together, these results indicate that CNF1 enhances HIF1α stabilization and VEGF secretion by activating RhoC in bladder cancer cells.

CNF1-induced RhoC activation modulates the stabilization of HIF1α by up-regulating HSF1-HSP90α

To explore how active RhoC promotes the stabilization of HIF1α, we compared the transcriptomes of T24 cells with CA-RhoC overexpression or vector control by RNA-Seq. We analyzed the genes associated with HIF1α degradation under hypoxic conditions (Fig. 4A). To verify some of the relevant upregulated genes in the RNA-seq data, qRT-PCR was performed (Fig. 4B). Among these genes, we found that the mRNA level of HSP90AA1 was significantly upregulated in CA-RhoC overexpressing cells. Western blotting analysis also revealed an increased protein level of HSP90α in CA-RhoC overexpressing T24 cells (Fig. 4C). We further validated the effects of CNF1 on HSP90α, which revealed that CNF1 also increased HSP90α expression (Fig. 4D). HSP90 can directly interact with HIF1α and promotes HIF1α stabilization under hypoxic conditions (22), which led us to examine whether HSP90α is involved in RhoC-facilitated HIF1α stabilization. We transfected T24 or 293T cells with HA-tagged HSP90α, MYC-tagged HIF1α and FLAG-tagged CA-RhoC or vector. Co-IP analysis indicated that CA-RhoC enhanced the interaction between HSP90α and HIF1α under hypoxic conditions (Fig. 4E, Supplementary Fig. 4A).

NF-κB and HSF1 were reported to regulate the expression of HSP90α (31). Ser326 phosphorylation is important for the transcriptional activity of HSF1 (31, 32). We found increased levels of HSF1 phosphorylated at Ser326, HSP90α and HIF1α after CA-RhoC overexpression (Fig. 4F, G) or CNF1 treatment (Fig. 4H), but there was no change in NF-κB activity (Supplementary Fig. 4B). We blocked HSF1 and NF-κB using commercial inhibitors (Fig. 4F, Supplementary Fig. 4C) and found that enhanced levels of phosphorylated HSF1, HSP90α and HIF1α were attenuated by inhibiting HSF1, but not by inhibiting NF-κB. To further confirm the role of HSF1 in promoting HSP90α and HIF1α levels, we knocked down HSF1 using specific siRNAs, and found that CA-RhoC or CNF1 induced HSF1 phosphorylation, HSP90α and

HIF1α increasement were not observed (Fig. 4G, H, Supplementary Fig. 4D).The effect of HSF1 on HIF1α in 5637 cells was also validated (Supplementary Fig. 4E). CNF1 effect on VEGF upregulation was not detected in T24 and 5637 cells with HSF1 knockdown (Fig. 4I, Supplementary Fig. 4F).

The above results demonstrate that CNF1 induced RhoC activation can increase HIF1α stabilization in bladder cancer cells through the HSF1-HSP90α axis.

Active RhoC promotes *in vivo* tumor-associated angiogenesis of bladder cancer

To determine if the *in vitro* observations could be replicated *in vivo*, the effect of RhoC activation on the angiogenesis mediated by bladder cancer cells was analyzed *in vivo* using a subcutaneous tumor mouse model. T24 cells were transduced with constitutively expressed CA-RhoC or the vector control. The expression of RhoC was confirmed in the transduced cells, and elevated HSP90α and HIF1α levels were also identified in T24 cells with CA-RhoC overexpression (Supplementary Fig. 4G). Five weeks after transplantation, we observed significantly elevated tumor growth in the CA-RhoC overexpression group compared with that in the control group (Fig. 5A and B). The tumor volume and weight were 3.6 and 2.4-fold higher than those in the control group (Fig. 5C and D). In addition, tumors in mice receiving the T24 cells with CA-RhoC had higher levels of HSP90α, HIF1α, and VEGF (Fig. 5E-H). We also found increased micro-vessel density (MVD) in tumors derived from the CA-RhoC-overexpressing T24 cells compared with those in the control group (Fig. 5I).

Overall, these results suggest that activation of RhoC by CNF1 promotes angiogenesis and tumor growth *in vivo*.

HSP90α, HIF1α and VEGF are implicated in advanced human bladder cancer

To identify the possible clinical correlations to our findings, the expression profiles of HSP90α , HIF1α and VEGF were analyzed by IHC staining using human tissue arrays containing 183 samples including 167 bladder carcinoma tissues of grade I, II, or III, 8 normal and 8 adjacent normal bladder tissues. We found that the levels of HSP90α , HIF1α and VEGF were strongly correlated with bladder cancer advanced

grades (Fig. 6A-D). Furthermore, the levels of their expression were correlated with each other (Fig. 6E-G). In addition, we performed the analysis using the integrated cancer microarray database, Oncomine (33), which revealed that HSP90AA1 (Fig. 6H) and HIF1A (Fig. 6I) mRNA levels are markedly upregulated in bladder cancer samples. We also analyzed the dataset from The Cancer Genome Atlas (TCGA) (34). The HSP90AA1 mRNA level (based on 407 bladder cancer samples) was significantly higher compared with the adjacent normal bladder tissues of 18 bladder cancer samples, and no difference was observed for HIF1A (Fig. 6J-K). However, both HSP90AA1 and HIF1A mRNA levels were found significantly increased in 18 bladder cancer samples compared with their paired adjacent normal bladder tissues (Fig. 6L-M). Furthermore, we performed the Kaplan-Meier survival analysis from the Gene Expression Profiling Interactive Analysis (GEPIA) web server (35). Elevated HIF1A expression is positively correlated with the poor survival in patients with bladder carcinoma, and a trend without statistical significance was observed for HSP90AA1 (Fig. 6N and O). We also analyzed published data from the GEO database (36). Analysis of two published clinical datasets (GSE83586 and GSE101723) revealed significantly positive correlations between the expression of HSP90AA1 and HIF1A in bladder cancer (Fig. 6P). Taken together, these observations support that the HSP90α-HIF1α-VEGF axis plays an important role in bladder cancer development.

Discussion

CNF1 has been reported to activate several Rho GTPases by deamidating specific glutamine residues (7). CNF1-mediated Rho GTPase activation changes cell function and contributes to many physiological and pathological processes. For example, CNF1 promotes bacterial invasion into host cells by activating Rac (37). Previously, we reported that CNF1 increased prostate cancer cell migration and invasion to promote prostate cancer metastasis through activating Cdc42 (6), and CNF1 reduced macrophage phagocytosis to induce inflammation during acute UTIs partially through Cdc42 (38). Schmidt reported that CNF1 enhanced breast cancer cell invasion through activating RhoC (39).

RhoC has been reported to play important roles in tumor progression, including angiogenesis (40-42), proliferation (43), invasion, and metastasis of tumors (11, 44). RhoC has been regarded as a new target for therapeutic vaccination against metastatic cancer (45). The mRNA and protein levels of RhoC are significantly higher in bladder cancer than in normal tissue (46). For bladder cancer, previous studies showed that RhoC was involved in its lung colonization (47), and the RhoC/ROCK pathway was closely associated with its invasion and metastasis (48). In addition, RhoC is correlated with the angiogenic component FGF2 in urothelial cell carcinoma of the bladder (49).

RhoC was shown to induce angiogenesis by regulating endothelial cell migration and organization (41), and to maintain vascular homeostasis by modulating endothelial cell proliferation and permeability (42). In addition, reports have shown that RhoC increases VEGF expression (40, 50-52). It was reported that p38 is involved in RhoC-induced VEGF production in breast cancer cells (52). However, the detailed specific mechanism through which RhoC accelerates VEGF secretion in bladder cancer remains unclear.

HIF1α stabilization is important for VEGF transcription, and several mechanisms, in addition to the classical pVHL pathway, have been reported to stabiliz HIF1α: (1)

HSP90 could directly interact with HIF1α and protect it from degradation (22); (2) increased expression of small ubiquitin-like modifier SUMO-1 under hypoxic conditions results in HIF1α SUMOylation and stabilization (53, 54); (3) USP20, a deubiquitinase, binds to HIF1α and subsequently removes ubiquitin from HIF1α, leading to its stabilization (55); and (4) YY1, a transcription factor, can directly bind to and stabilizing HIF1α (56). In the present study, we examined the transcription of factors associated with HIF1α stabilization and identified that activated RhoC induced HIF1α stabilization and VEGF production by increasing HSP90α expression and the interaction between HIF1α and HSP90.

ACKNOWLEDGMENTS

This study was supported by grants from the National Natural Science Foundation of China (NSFC) Programs (31970133, 81672740, 81572882, 31670071), the National Key Technologies R&D Program, Intergovernmental international innovation cooperation (2018YFE0102000), the Science & Technology Development Fund of Tianjin Education Commission for Higher Education (2017ZD12), Tianjin Science and Technology Commissioner Project (18JCZDJC36000).

AUTHOR CONTRIBUTIONS

QW, ZY and ZZ designed the study, YG, JW, KZ, JL, LW, and SG performed the majority of experiments. QW, ZY, YG, ZZ and ETK analyzed the data and wrote the paper. All authors discussed the data, and reviewed the manuscript.

References

1. Bien, J., Sokolova, O., and Bozko, P. (2012) Role of Uropathogenic *Escherichia coli* Virulence Factors in Development of Urinary Tract Infection and Kidney Damage. *Int. J. Nephrol.* **2012**, 681473
2. Nielubowicz, G. R., and Mobley, H. L. (2010) Host-pathogen interactions in urinary tract infection. *Nat. Rev. Urol.* **7**, 430-441
3. Mitsumori, K., Terai, A., Yamamoto, S., Ishitoya, S., and Yoshida, O. (1999) Virulence characteristics of *Escherichia coli* in acute bacterial prostatitis. *J. Infect. Dis.* **180**, 1378-1381
4. Tolg, C., Sabha, N., Cortese, R., Panchal, T., Ahsan, A., Soliman, A., Aitken, K. J., Petronis, A., and Bagli, D. J. (2011) Uropathogenic *E. coli* infection provokes epigenetic downregulation of CDKN2A (p16INK4A) in uroepithelial cells. *Lab. Invest.* **91**, 825-836
5. Simons, B. W., Durham, N. M., Bruno, T. C., Grosso, J. F., Schaeffer, A. J., Ross, A. E., Hurley, P. J., Berman, D. M., Drake, C. G., Thumbikat, P., and Schaeffer, E. M. (2015) A human prostatic bacterial isolate alters the prostatic microenvironment and accelerates prostate cancer progression. *J. Pathol.* **235**, 478-489
6. Guo, Y., Zhang, Z., Wei, H., Wang, J., Lv, J., Zhang, K., Keller, E. T., Yao, Z., and Wang, Q. (2017) Cytotoxic necrotizing factor 1 promotes prostate cancer progression through activating the Cdc42-PAK1 axis. *J. Pathol.* **243**, 208-219
7. Schmidt, G., Sehr, P., Wilm, M., Selzer, J., Mann, M., and Aktories, K. (1997) Gln 63 of Rho

is deamidated by *Escherichia coli* cytotoxic necrotizing factor-1. *Nature* **387**, 725-729

8. Vega, F. M., and Ridley, A. J. (2008) Rho GTPases in cancer cell biology. *FEBS Lett.* **582**, 2093-2101

9. Gomez del Pulgar, T., Benitah, S. A., Valeron, P. F., Espina, C., and Lacal, J. C. (2005) Rho GTPase expression in tumourigenesis: evidence for a significant link. *Bioessays* **27**, 602-613

10. Karlsson, R., Pedersen, E. D., Wang, Z., and Brakebusch, C. (2009) Rho GTPase function in tumorigenesis. *Biochim. Biophys. Acta* **1796**, 91-98

11. Clark, E. A., Golub, T. R., Lander, E. S., and Hynes, R. O. (2000) Genomic analysis of metastasis reveals an essential role for RhoC. *Nature* **406**, 532-535

12. Golen, K. L., Wu, Z. F., Qiao, X. T., Bao, L., and Merajver, S. D. (2000) RhoC GTPase overexpression modulates induction of angiogenic factors in breast cells. *Neoplasia* **2**, 418-425

13. Yang, J., Wang, Q., Qiao, C., Lin, Z., Li, X., Huang, Y., Zhou, T., Li, Y., Shen, B., Lv, M., and Feng, J. (2014) Potent anti-angiogenesis and anti-tumor activity of a novel human anti-VEGF antibody, MIL60. *Cell. Mol. Immunol.* **11**, 285-293

14. Folkman, J. (1971) Tumor angiogenesis: therapeutic implications. *N. Engl. J. Med.* **285**, 1182-1186

15. Ferrara, N., Gerber, H. P., and LeCouter, J. (2003) The biology of VEGF and its receptors. *Nat. Med.* **9**, 669-676

16. Semenza, G. L. (2000) Hypoxia, clonal selection, and the role of HIF-1 in tumor progression. *Crit. Rev. Biochem. Mol. Biol.* **35**, 71-103

17. Semenza, G. L. (2000) HIF-1: mediator of physiological and pathophysiological responses to hypoxia. *J. Appl. Physiol. (1985)* **88**, 1474-1480

18. Semenza, G. L. (2003) Targeting HIF-1 for cancer therapy. *Nat Rev Cancer* **3**, 721-732

19. Yu, F., White, S. B., Zhao, Q., and Lee, F. S. (2001) HIF-1alpha binding to VHL is regulated by stimulus-sensitive proline hydroxylation. *Proc. Natl. Acad. Sci. U S A* **98**, 9630-9635

20. Tanimoto, K., Makino, Y., Pereira, T., and Poellinger, L. (2000) Mechanism of regulation of the hypoxia-inducible factor-1 alpha by the von Hippel-Lindau tumor suppressor protein. *EMBO J.* **19**, 4298-4309

21. Epstein, A. C., Gleadle, J. M., McNeill, L. A., Hewitson, K. S., O'Rourke, J., Mole, D. R.,

Mukherji, M., Metzen, E., Wilson, M. I., Dhanda, A., Tian, Y. M., Masson, N., Hamilton, D. L., Jaakkola, P., Barstead, R., Hodgkin, J., Maxwell, P. H., Pugh, C. W., Schofield, C. J., and Ratcliffe, P. J. (2001) C. elegans EGL-9 and mammalian homologs define a family of dioxygenases that regulate HIF by prolyl hydroxylation. *Cell* **107**, 43-54

22. Jochmanova, I., Yang, C., Zhuang, Z., and Pacak, K. (2013) Hypoxia-inducible factor signaling in pheochromocytoma: turning the rudder in the right direction. *J. Natl. Cancer Inst.* **105**, 1270-1283

23. Yee Koh, M., Spivak-Kroizman, T. R., and Powis, G. (2008) HIF-1 regulation: not so easy come, easy go. *Trends Biochem. Sci.* **33**, 526-534

24. Shen, K. H., Li, C. F., Chien, L. H., Huang, C. H., Su, C. C., Liao, A. C., and Wu, T. F. (2016) Role of galectin-1 in urinary bladder urothelial carcinoma cell invasion through the JNK pathway. *Cancer Sci.* **107**, 1390-1398

25. Cathcart, J., Pulkoski-Gross, A., and Cao, J. (2015) Targeting Matrix Metalloproteinases in Cancer: Bringing New Life to Old Ideas. *Genes Dis.* **2**, 26-34

26. Matsumoto, K., and Ema, M. (2014) Roles of VEGF-A signalling in development, regeneration, and tumours. *J. Biochem.* **156**, 1-10

27. Majmundar, A. J., Wong, W. J., and Simon, M. C. (2010) Hypoxia-inducible factors and the response to hypoxic stress. *Mol. Cell* **40**, 294-309

28. Carmeliet, P., and Jain, R. K. (2000) Angiogenesis in cancer and other diseases. *Nature* **407**, 249-257

29. Semenza, G. L. (2002) HIF-1 and tumor progression: pathophysiology and therapeutics. *Trends Mol. Med.* **8**, S62-67

30. Fabbri, A., Travaglione, S., and Fiorentini, C. (2010) Escherichia coli cytotoxic necrotizing factor 1 (CNF1): toxin biology, in vivo applications and therapeutic potential. *Toxins (Basel)* **2**, 283-296

31. Prodromou, C. (2016) Mechanisms of Hsp90 regulation. *Biochem. J.* **473**, 2439-2452

32. Boellmann, F., Guettouche, T., Guo, Y., Fenna, M., Mnayer, L., and Voellmy, R. (2004) DAXX interacts with heat shock factor 1 during stress activation and enhances its transcriptional activity. *Proc. Natl. Acad. Sci. U S A* **101**, 4100-4105

33. Rhodes, D. R., Kalyana-Sundaram, S., Mahavisno, V., Varambally, R., Yu, J., Briggs, B. B.,

Barrette, T. R., Anstet, M. J., Kincead-Beal, C., Kulkarni, P., Varambally, S., Ghosh, D., and Chinnaiyan, A. M. (2007) Oncomine 3.0: genes, pathways, and networks in a collection of 18,000 cancer gene expression profiles. *Neoplasia* **9**, 166-180

34. Lee, J.-S. (2016) Exploring cancer genomic data from the cancer genome atlas project. *BMB Rep.* **49**, 607-611

35. Tang, Z., Li, C., Kang, B., Gao, G., Li, C., and Zhang, Z. (2017) GEPIA: a web server for cancer and normal gene expression profiling and interactive analyses. *Nucleic Acids Res.* **45**, W98-w102

36. Clough, E., and Barrett, T. (2016) The Gene Expression Omnibus Database. *Methods Mol. Biol.* **1418**, 93-110

37. Doye, A., Mettouchi, A., Bossis, G., Clement, R., Buisson-Touati, C., Flatau, G., Gagnoux, L., Piechaczyk, M., Boquet, P., and Lemichez, E. (2002) CNF1 exploits the ubiquitin-proteasome machinery to restrict Rho GTPase activation for bacterial host cell invasion. *Cell* **111**, 553-564

38. Yang, H., Li, Q., Wang, C., Wang, J., Lv, J., Wang, L., Zhang, Z. S., Yao, Z., and Wang, Q. (2018) Cytotoxic Necrotizing Factor 1 Downregulates CD36 Transcription in Macrophages to Induce Inflammation During Acute Urinary Tract Infections. *Front. Immunol.* **9**, 1987

39. Lang, S., Busch, H., Boerries, M., Brummer, T., Timme, S., Lassmann, S., Aktories, K., and Schmidt, G. (2017) Specific role of RhoC in tumor invasion and metastasis. *Oncotarget* **8**, 87364-87378

40. Zhao, Z. H., Tian, Y., Yang, J. P., Zhou, J., and Chen, K. S. (2015) RhoC, vascular endothelial growth factor and microvascular density in esophageal squamous cell carcinoma. *World J. Gastroenterol.* **21**, 905-912

41. Wang, W., Wu, F., Fang, F., Tao, Y., and Yang, L. (2008) RhoC is essential for angiogenesis induced by hepatocellular carcinoma cells via regulation of endothelial cell organization. *Cancer Sci.* **99**, 2012-2018

42. Hoeppner, L. H., Sinha, S., Wang, Y., Bhattacharya, R., Dutta, S., Gong, X., Bedell, V. M., Suresh, S., Chun, C., Ramchandran, R., Ekker, S. C., and Mukhopadhyay, D. (2015) RhoC maintains vascular homeostasis by regulating VEGF-induced signaling in endothelial cells. *J. Cell Sci.* **128**, 3556-3568

43. Wu, Y., Tao, Y., Chen, Y., and Xu, W. (2012) RhoC regulates the proliferation of gastric

cancer cells through interaction with IQGAP1. *PLoS One* **7**, e48917

44. Liu, N., Zhang, G., Bi, F., Pan, Y., Xue, Y., Shi, Y., Yao, L., Zhao, L., Zheng, Y., and Fan, D. (2007) RhoC is essential for the metastasis of gastric cancer. *J. Mol. Med. (Berl)* **85**, 1149-1156

45. Wenandy, L., Sorensen, R. B., Svane, I. M., Thor Straten, P., and Andersen, M. H. (2008) RhoC a new target for therapeutic vaccination against metastatic cancer. *Cancer Immunol. Immunother.* **57**, 1871-1878

46. Volanis, D., Zaravinos, A., Kadiyska, T., Delakas, D., Zoumpourlis, V., and Spandidos, D. A. (2011) Expression profile of Rho kinases in urinary bladder cancer. *J. Buon* **16**, 511-521

47. Griner, E. M., Dancik, G. M., Costello, J. C., Owens, C., Guin, S., Edwards, M. G., Brautigan, D. L., and Theodorescu, D. (2015) RhoC Is an Unexpected Target of RhoGDI2 in Prevention of Lung Colonization of Bladder Cancer. *Mol. Cancer Res.* **13**, 483-492

48. Kamai, T., Tsujii, T., Arai, K., Takagi, K., Asami, H., Ito, Y., and Oshima, H. (2003) Significant association of Rho/ROCK pathway with invasion and metastasis of bladder cancer. *Clin. Cancer Res.* **9**, 2632-2641

49. Zaravinos, A., Volanis, D., Lambrou, G. I., Delakas, D., and Spandidos, D. A. (2012) Role of the angiogenic components, VEGFA, FGF2, OPN and RHOC, in urothelial cell carcinoma of the urinary bladder. *Oncol. Rep.* **28**, 1159-1166

50. Xie, S., Zhu, M., Lv, G., Geng, Y., Chen, G., Ma, J., and Wang, G. (2013) Overexpression of Ras homologous C (RhoC) induces malignant transformation of hepatocytes *in vitro* and in nude mouse xenografts. *PLoS One* **8**, e54493

51. Zhao, Y., Zong, Z. H., and Xu, H. M. (2010) RhoC expression level is correlated with the clinicopathological characteristics of ovarian cancer and the expression levels of ROCK-I, VEGF, and MMP9. *Gynecol. Oncol.* **116**, 563-571

52. Golen, K. L., Bao, L. W., Pan, Q., Miller, F. R., Wu, Z. F., and Merajver, S. D. (2002) Mitogen activated protein kinase pathway is involved in RhoC GTPase induced motility, invasion and angiogenesis in inflammatory breast cancer. *Clin. Exp. Metastasis* **19**, 301-311

53. Shao, R., Zhang, F. P., Tian, F., Anders Friberg, P., Wang, X., Sjoland, H., and Billig, H. (2004) Increase of SUMO-1 expression in response to hypoxia: direct interaction with HIF-1alpha in adult mouse brain and heart *in vivo*. *FEBS Lett.* **569**, 293-300

54. Bae, S. H., Jeong, J. W., Park, J. A., Kim, S. H., Bae, M. K., Choi, S. J., and Kim, K. W. (2004) Sumoylation increases HIF-1alpha stability and its transcriptional activity. *Biochem. Biophys. Res. Commun.* **324**, 394-400

55. Li, Z., Wang, D., Messing, E. M., and Wu, G. (2005) VHL protein-interacting deubiquitinating enzyme 2 deubiquitinates and stabilizes HIF-1alpha. *EMBO Rep.* **6**, 373-378

56. Wu, S., Kasim, V., Kano, M. R., Tanaka, S., Ohba, S., Miura, Y., Miyata, K., Liu, X., Matsuhashi, A., Chung, U. I., Yang, L., Kataoka, K., Nishiyama, N., and Miyagishi, M. (2013) Transcription factor YY1 contributes to tumor growth by stabilizing hypoxia factor HIF-1alpha in a p53-independent manner. *Cancer Res.* **73**, 1787-1799

Figure legends

Figure 1. CNF1 promotes the migration and invasion of bladder cancer cells and vascular endothelial cells.

Transwell-based migration and invasion assays of T24 cells (A, B) and HUVECs (D, E) treated with 1 nmol/L recombinant CNF1 protein, PBS, and the inactivated CNF1 mutant C866S (n = 3, three independent experiments). (C) Zymography assay of

MMP2 activities in 5637 cells treated with PBS and 1 nmol/L CNF1 (n = 3, three independent experiments). β-Actin was loaded as an internal control. Data are the mean ± SD. *p < 0.05, **p < 0.01; one-way ANOVA (A, B, D, and E) or Student's *t*-test (C). Scale bar = 50 μm.

Figure 2. CNF1 induces VEGF secretion in bladder cancer cells by promoting HIF1α stabilization and subsequently promotes angiogenesis.

(A) The T24 cells were incubated with CNF1 (3 nmol/L) for 24 h under normoxic or hypoxic conditions, and VEGF secretion in the culture medium was analyzed by ELISA (n = 3, three independent experiments). (B, C) Time- and concentration-dependent VEGF secretion in T24 cells treated by CNF1 (3 nmol/L) under hypoxic conditions (n = 3, three independent experiments). (D) The T24 cells were stimulated with CNF1 (3 nmol/L) or PBS for 36 h. The medium was collected and then applied to HUVECs for 6 h. The capillary-like structure formation in HUVECs was examined using a tube formation assay (n = 3, three independent experiments). Tube formation ability was visualized and calculated by measuring the length of the tubes. (E) T24 cells were incubated with CNF1 (3 nmol/L) for 24 h under hypoxic conditions, and VEGF expression was examined by qPCR (n = 3, three independent experiments). (F) Western blotting analysis of HIF1α in T24 cells after treatment with CNF1 (3 nmol/L) under hypoxic conditions for 24 h, with PBS, dialysis buffer, LPS (1.26×10^{-3} ng/ml) and C866S treatments as controls. (G) T24 cells were pretreated with the proteasome inhibitor MG132 (10 μmol/L) for 1 h followed by stimulation with CNF1 (3 nmol/L) for 24 h under normoxic or hypoxic conditions, and HIF1α expression was analyzed by western blotting. (H) Western blotting analysis of HIF1α in 3 nmol/L CNF1-treated T24 cells transfected with scrambled or HIF1A siRNA under hypoxic conditions. (I) T24 cells were transfected with scrambled or HIF1A siRNA for 24 h followed by stimulation with CNF1 (3 nmol/L) or PBS for 36 h. VEGF secretion in culture medium was examined by ELISA (n = 3, three independent experiments). (J) The same medium as described in (I) was applied to HUVECs for 6 h. The capillary-like structure formation in HUVECs was examined using a tube formation assay (n = 3, three independent experiments). Data are the mean ± SD. *p < 0.05, **p

< 0.01; one-way ANOVA (A-C, I and J) or Student's *t*-test (D, E). Scale bar = 100 μm.

Figure 3. CNF1 modulates the expression of HIF1α and the secretion of VEGF by activating RhoC in bladder cancer cells.

(A) T24 cells were transfected with a scrambled control siRNA or those targeting respective Rho GTPase siRNAs for 24 h, followed by stimulation with PBS or CNF1 (3 nmol/L) for another 24 h under hypoxic conditions, and HIF1α expression was examined by western blotting. (B) T24 cells were incubated with PBS or CNF1 for 3 to 36 h and mobility-shifting was examined by electrophoresis. (C) Western blotting analysis of activated RhoC in T24 cells treated with recombinant CNF1 protein (3 nmol/L) or PBS for 24 h after immunoprecipitation with GTP pull-down assays using anti-RhoC antibody. (D) Western blotting analysis of T24 cells transfected with vector, wild-type RhoC, or constitutively active RhoC (Q63E) under hypoxic conditions. (E) T24 cells were transfected with vector, wild-type RhoC, or Q63E for 48 h, and VEGF secretion in the culture medium was examined by ELISA (n = 3, three independent experiments). (F) T24 cells were transfected with scrambled or RhoC siRNA for 24 h followed by stimulation with CNF1 protein (3 nmol/L) or PBS for 24 h, and VEGF secretion in culture medium was examined by ELISA (n = 3, three independent experiments). Data are the mean ± SD. *p < 0.05, **p < 0.01; one-way ANOVA (E, F).

Figure 4. CNF1 induced RhoC activation modulates the HIF1α stabilization by up-regulating HSF1- HSP90α interaction.

(A) Heatmap of the HIF1α degradation-related gene expression levels detected by RNA-seq in T24 cells stably expressing the RhoC constitutively active mutant Q63E or vector under hypoxic condition. (B) qRT-PCR confirmation of the up-regulated genes expression profile under hypoxic condition (n = 3, three independent experiments). (C) Western blotting analysis of T24 cells transduced with vector and Q63E under hypoxic condition. (D) Western blotting analysis of T24 cells treated with 1 nmol/L CNF1. (E) T24 cells were transfected with combinations of MYC-HIF1α, HA-HSP90α and FLAG-RhoC-Q63E under normoxic or hypoxic

condition. Protein extracts from the transfected cells were subjected to IP with antibody against MYC and analyzed by immunoblotting with the indicated antibodies. (F) Analysis of phosphorylated HSF1, total HSF1, HSP90α and HIF1α in transduced T24 cells treated with the HSF1 inhibitor KRIBB11 (10 μmol/L), or with DMSO as the control under hypoxic condition. (G-H) Western blotting analysis of transduced T24 cells (G) and 1 nmol/L CNF1 treated T24 cells (H) subject to siRNAs targeting HSF1 and scrambled non-targeting control siRNA under hypoxic conditions. (I) T24 cells were transfected with scrambled or HSF1 siRNA for 24 h followed by stimulation with CNF1 (3 nmol/L) or PBS for 24 h under hypoxic condition, and VEGF secretion in culture medium was examined by ELISA (n = 3, three independent experiments). Data are the mean ± SD. **p < 0.01; one-way ANOVA (B, I).

Figure 5. Active RhoC promotes the tumor-associated angiogenesis of bladder cancer *in vivo*.

(A) Morphological images of tumor xenografts resected from nude mice injected with T24 cells transduced with vector (VEC) or constitutively active mutant of RhoC (Q63E) after 5 weeks in each group. (B) Tumor growth in nude mice with Q63E or VEC T24 cells subcutaneously injected into their flanks (n = 9, two independent experiments). Tumor volumes were determined by direct measurement using a caliper and calculated using the formula: (widest diameter × smallest diameter^2)/2. Tumor volume (C) and weight (D) of xenograft nude mice injected with Q63E or VEC T24 cells in the xenograft model (n = 9, two independent experiments). (E-H) Immunohistochemical analysis of RhoC, HSP90α , HIF1α, or VEGF expression in murine tumors. (I) Immunofluorescence analysis of $CD31^+$ blood vessels in murine tumors (n = 3, three independent experiments each with multiple fields). Data are the mean ± SD. *p < 0.05, **p < 0.01; non-parametric Mann-Whitney test (B, C, D and I). Scale bar = 50 μm (E-H) or 100 μm (I).

Figure 6. HSP90α , HIF1α, and VEGF expressions are positively correlated with advanced human bladder cancer.

(A) IHC analysis of HSP90α, HIF1α and VEGF using human bladder cancer tissue

microarray. Representative images (original magnification 200×) from normal bladder tissues, adjacent normal bladder tissues, and malignant bladder tissues at different stages are shown. (B-D) Mean intensity of staining of HSP90α (B), HIF1α (C) and VEGF (D) were determined by Image-Pro Plus software and presented with box plots. (E-G) The correlation coefficient and *P* values were analyzed as indicated. (H-I) Analysis of Sanchez-Carbayo bladder from Oncomine for the expression of HSP90AA1 (H) and HIF1A (I) in normal human bladder tissues and bladder carcinoma samples. (J-K) Analysis of the mRNA level of HSP90AA1 (J) and HIF1A (K) in 407 bladder cancer and 18 adjacent normal bladder tissues obtained from the TCGA database. (L-M) Analysis of TCGA data set for the mRNA expression of HSP90AA1 (L) and HIF1A (M) in 18 bladder cancer samples and the paired adjacent normal bladder tissues. (N-O) Kaplan-Meier survival analysis for the relationship between the survival of bladder cancer patients and expression levels of HSP90AA1 (N) and HIF1A (O) mRNA using the online tool (http://gepia.cancer-pku.cn/). (P) Analysis of public datasets (GSE83586, GSE101723) for the expression of HIF1A and HSP90AA1 in bladder cancer. The relative levels of HSP90AA1 were plotted against that of HIF1A. Data are presented with box plots. *P < 0.05, **P < 0.01; one-way ANOVA (B-D); Pearson's correlation coefficient and Spearman's correlation coefficient (E-G, P); unpaired, 2-tailed Student's *t*-test (H-K); paired, 2-tailed Student's *t*-test (L, M) or log rank test (N, O).

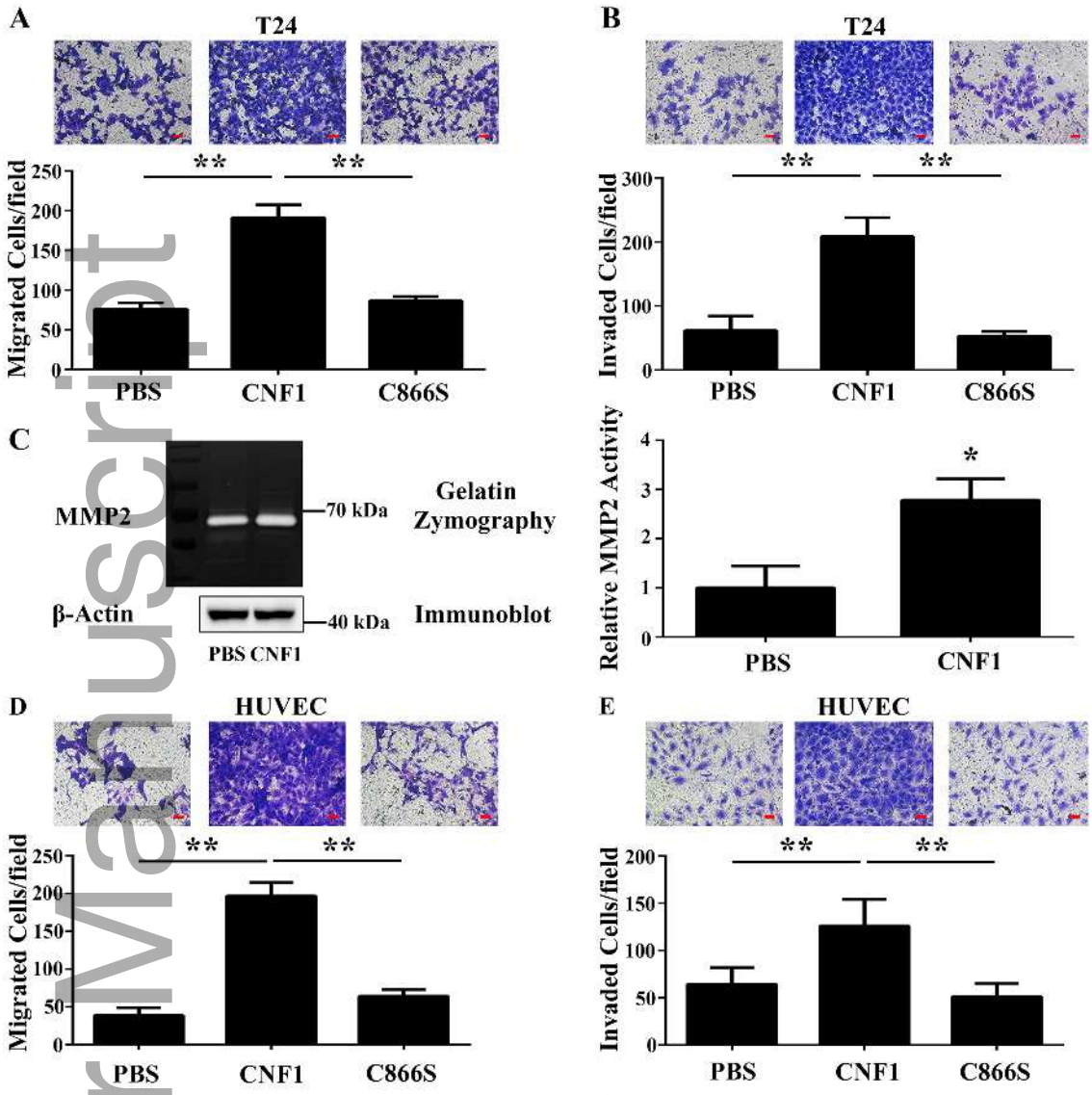

Figure 1

fsb2_20522_f1.tif

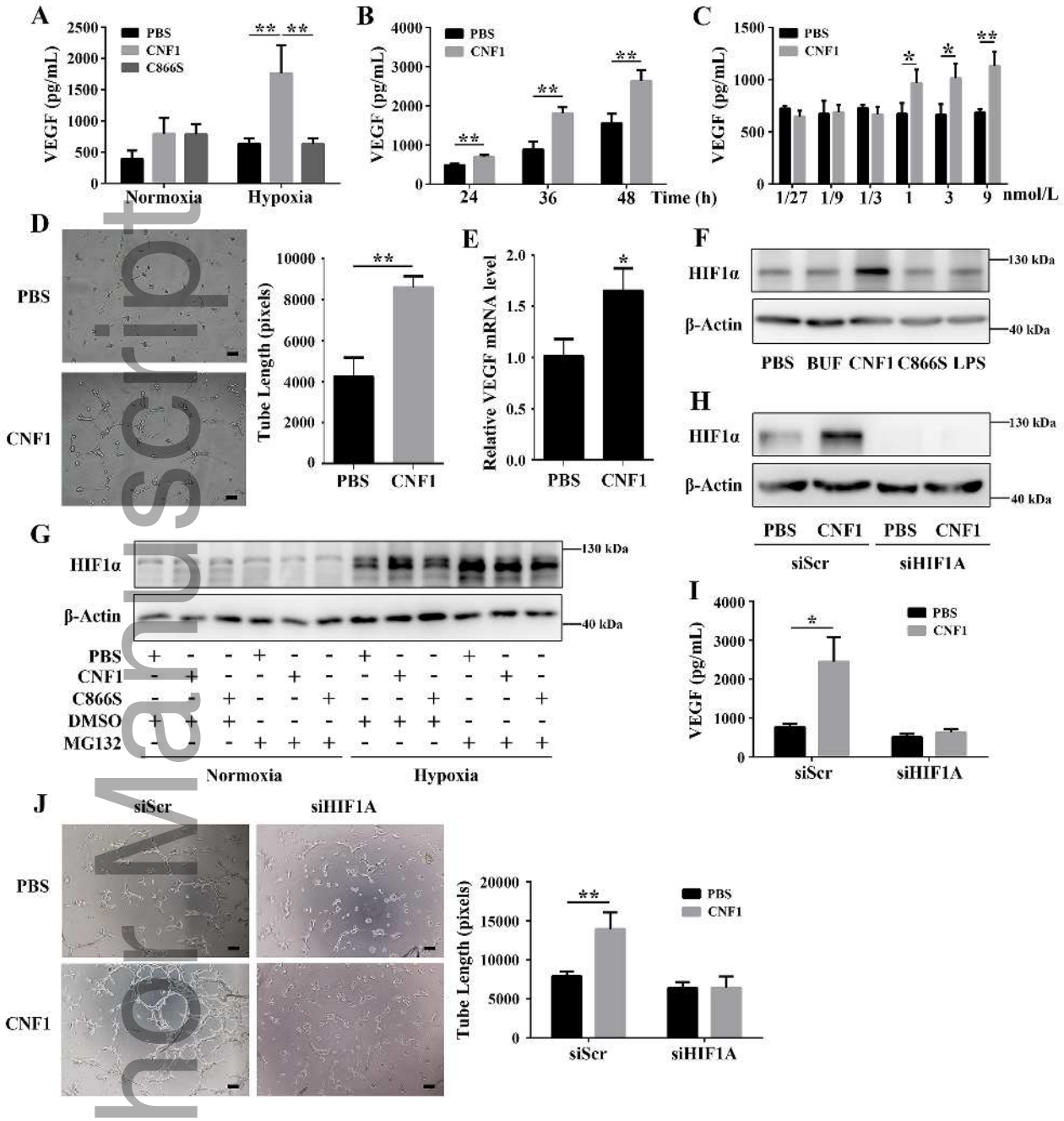

Figure 2

fsb2_20522_f2.tif

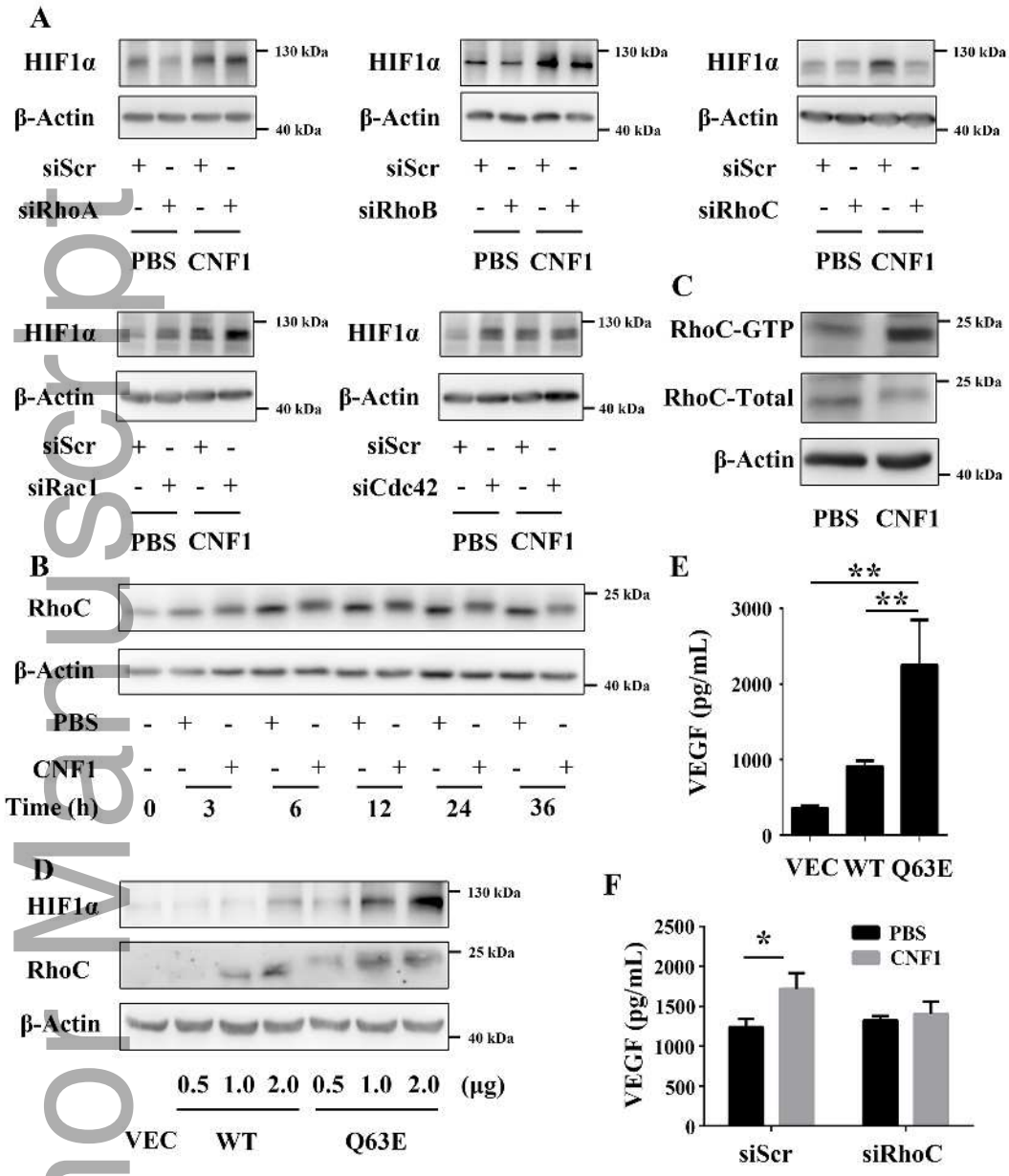

Figure 3

fsb2_20522_f3.tif

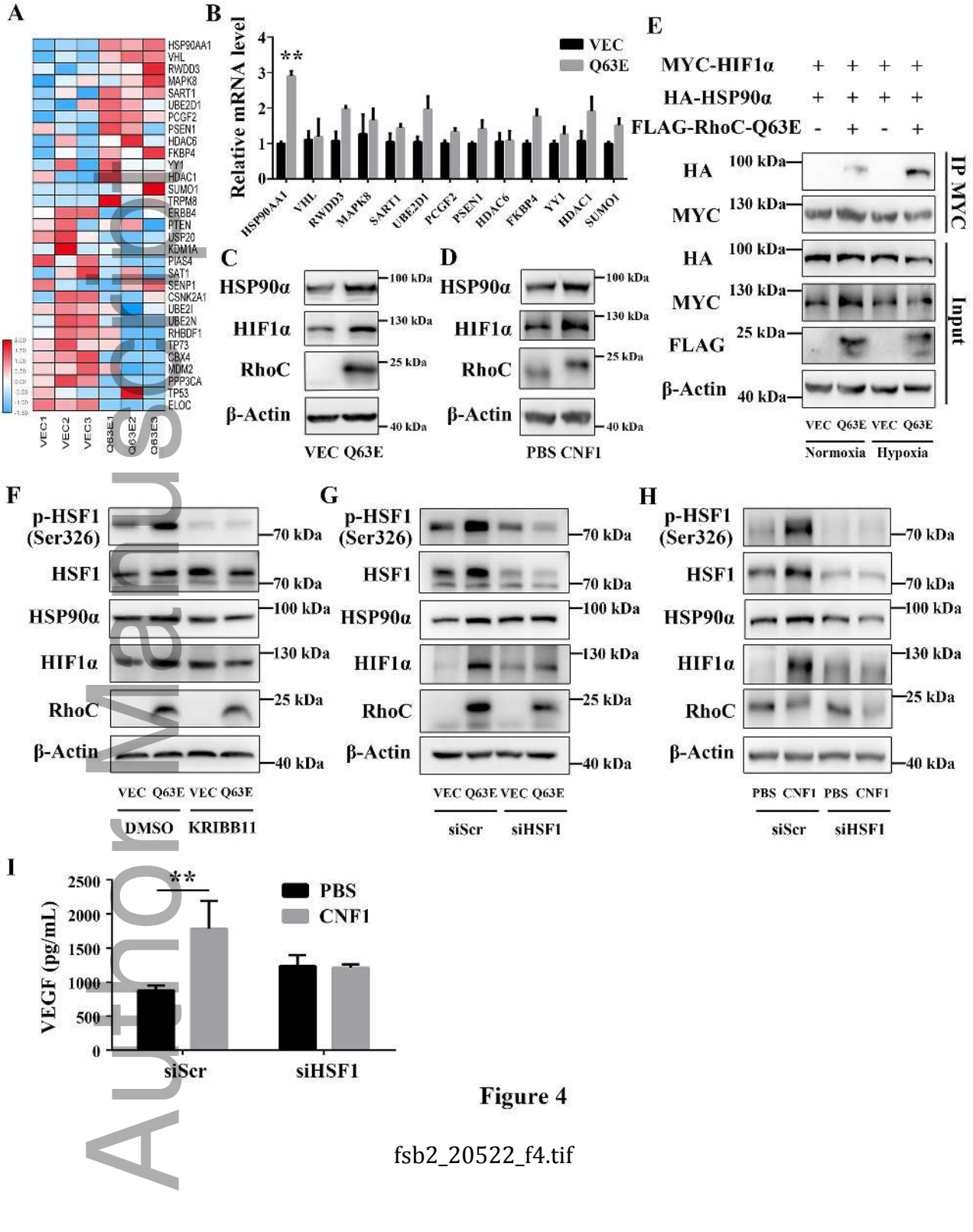

Figure 4

fsb2_20522_f4.tif

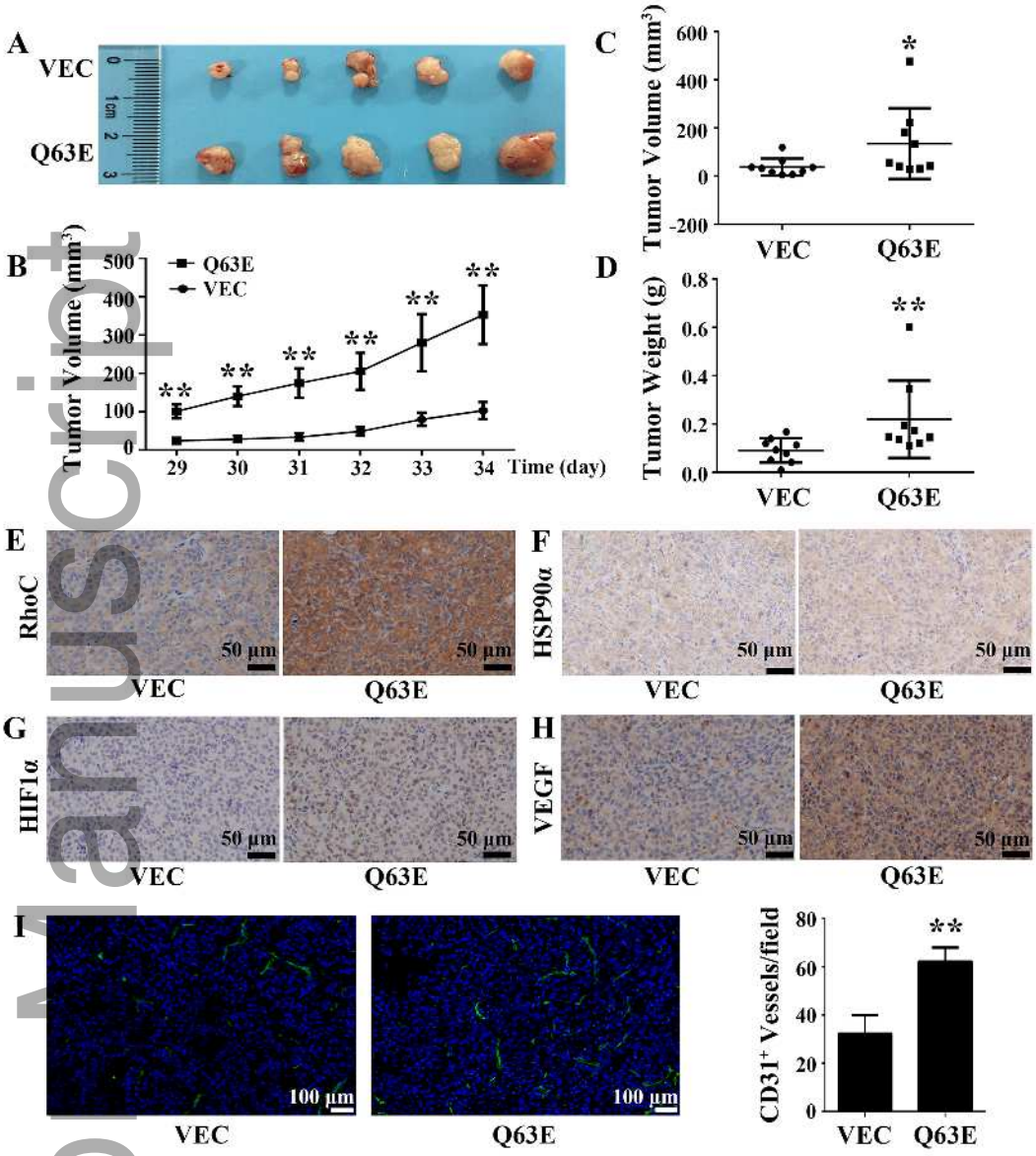

Figure 5

fsb2_20522_f5.tif

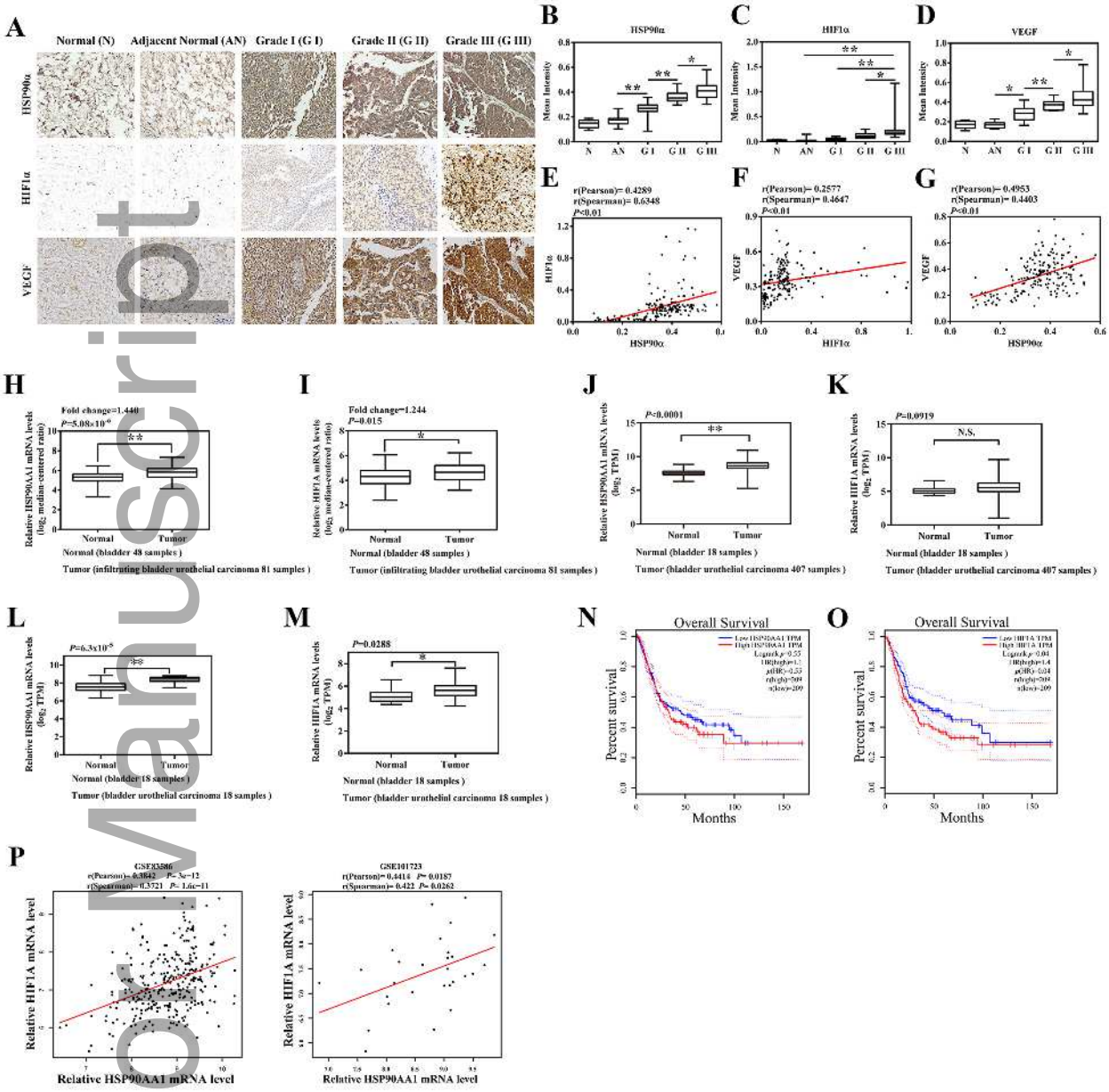

Figure 6

fsb2_20522_f6.tif